

Pearcey-Inspired Quartic Wavefront Shaping for Obstructed Near-Field Multi-User Communications

Yifeng Qin, *Member, IEEE*, Jing Chen, and Zhi Hao Jiang, *Member, IEEE*

Abstract—Radiative near-field (RNF) beamforming is vulnerable to blockages that disrupt Fresnel zones. This letter proposes an obstruction-unaware wavefront shaping strategy inspired by catastrophe optics. By superimposing a calibrated quartic phase, we generate a Pearcey-like wave packet that exhibits structural stability against perturbations. We establish a fair comparison protocol where the quartic beam is calibrated in free space to avoid exploiting obstruction knowledge. Numerical results demonstrate up to 8.5 dB SINR gain over conventional focusing for multi-user scenarios near the depth-of-focus limit. Crucially, this gain stems from improved channel conditioning under partial blockage, which mitigates the severe noise amplification inherent to zero-forcing precoding.

Index Terms—Radiative near-field (RNF), wavefront shaping, Pearcey function, zero-forcing (ZF), blockage mitigation.

I. INTRODUCTION

THE evolution toward 6G networks has spurred significant interest in extremely large-scale antenna arrays (ELAA) operating in the radiative near-field (RNF) region [1], [2]. Unlike the planar wavefronts assumed in far-field communications, the spherical wavefronts in the RNF region enable beam focusing at specific locations, unlocking the range dimension for spatial multiplexing [3]. This capability allows a base station (BS) to serve multiple users located at the same angle but different distances, effectively mitigating multi-user interference (MUI) through range-division multiple access.

However, the theoretical gains of RNF focusing are highly sensitive to the propagation environment. In practical scenarios, line-of-sight (LoS) paths are frequently partially blocked by finite obstructions (e.g., lamp posts, human bodies, or vehicles). While complete blockage is detrimental, partial blockage—diffraction by finite obstacles—induces amplitude fluctuations and phase distortions [4]. In multi-user (MU) systems, this is particularly critical: even minor distortions can destroy the orthogonality between users' channel vectors. When users are closely spaced, specifically near the *range separability limit* (governed by the array's depth-of-focus), such obstructions cause the channel matrix condition number to spike. Consequently, standard zero-forcing (ZF) precoding suffers from severe noise amplification, drastically reducing the sum rate [5].

Existing solutions to enhance robustness often rely on obtaining channel state information (CSI) of the obstruction [6]

or deploying reconfigurable intelligent surfaces (RIS) to bypass blockages [7], [8]. Alternatively, diffraction-free beams, such as Bessel [9], [10], [11] and Airy beams [12], [13], [14], [15] have been explored for their self-healing properties. However, Bessel beams cannot effectively focus energy on a specific target user in the near-field regime due to their energy distribution along the propagation axis, while Airy beams are primarily effective for half-space obstacle scenarios [13] rather than the finite on-axis obstructions encountered in dense deployments. More importantly, most prior works focus on maintaining the power of a single link, rather than optimizing the *joint condition number* of a multi-user channel matrix under blind obstruction scenarios.

In this letter, we propose a Pearcey-inspired quartic wavefront shaping strategy for RNF MU communications. Drawing from catastrophe optics [16], we exploit the Pearcey integral, which inherently contains a quartic phase term. Physically, unlike the standard focal point which is structurally unstable and sensitive to aperture truncation, the Pearcey cusp caustic exhibits structural stability [17]. This implies that its qualitative intensity pattern is resilient to perturbations, such as those introduced by finite obstructions. We demonstrate that by superimposing a calibrated quartic phase onto the conventional focusing phase, the resulting beam inherits this resilience. Consequently, it mitigates the ill-conditioning of the multi-user channel matrix caused by partial blockage, stabilizing the ZF inversion without requiring obstruction CSI.

Our contributions are as follows:

- 1) We establish an obstruction-unaware fair comparison protocol between conventional near-field focusing and Pearcey-inspired quartic shaping, where beam calibration is performed in free space only to avoid “peeking” at the obstruction.
- 2) We introduce two universal dimensionless parameters, W_{obs}/r_F and $\mu = \Delta z/\Delta z_{\text{DoF}}$, and provide an advantage regime map in terms of ZF common-SINR gain.
- 3) We reveal the physical mechanism of the SINR gain: the structural stability of the Pearcey wavefront mitigates the ill-conditioning of the multi-user channel matrix, which outweighs the intrinsic focal-gain penalty in obstructed regimes.

II. SYSTEM MODEL AND PROPAGATION ANALYSIS

A. System Geometry and Physical Scaling

Consider a radiative near-field (RNF) downlink scenario in a two-dimensional xz -plane. A Base Station (BS) is equipped with a Uniform Linear Array (ULA) located on the x -axis

This work was supported by ... (Corresponding author: Yifeng Qin)
Y. Qin and J. Chen are with the Peng Cheng Laboratory, Shenzhen, 518052, China (e-mails: ee06b147@gmail.com, chenj12@pcl.ac.cn).

Z. H. Jiang is with the State Key Laboratory of Millimeter Waves, School of Information Science and Engineering, Southeast University, Nanjing 210096, China (e-mail: zhihao.jiang@seu.edu.cn).

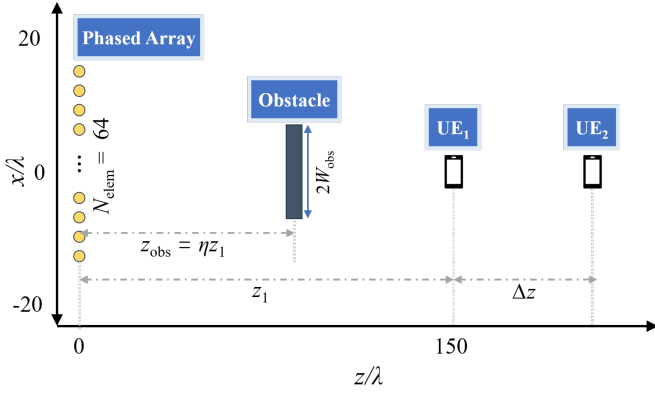


Fig. 1. System geometry illustrating the ULA with aperture $D = N_{\text{elem}}d$, the two co-angular users UE_1 and UE_2 separated by Δz , and the finite obstruction of width $2W_{\text{obs}}$ located at z_{obs} .

at $z = 0$. The array consists of $N_{\text{elem}} = 64$ elements with inter-element spacing $d = 0.49\lambda$, resulting in a total physical aperture $D = N_{\text{elem}}d \approx 31\lambda$.

The system serves two single-antenna users, denoted as UE_1 and UE_2 , located along the array's normal direction (the z -axis). As illustrated in Fig. 1, UE_1 is located at $(0, z_1)$, and UE_2 is located at $(0, z_2)$, where $z_2 = z_1 + \Delta z$. Here, $\Delta z > 0$ denotes the range separation between the users.

A finite obstruction is located at a distance $z_{\text{obs}} = \eta z_1$ ($0 < \eta < 1$) from the BS, parallel to the ULA. This obstruction is modeled as an opaque strip centered on the propagation axis with a physical half-width W_{obs} (total width $2W_{\text{obs}}$).

To ensure fair comparisons and maintain physical generality, we characterize the system using two universal dimensionless parameters.

1) *Fresnel Radius at Obstruction*: The diffraction patterns induced by the finite obstruction are fundamentally governed by the size of the obstruction relative to the Fresnel zone at that distance. We define the first Fresnel zone radius as:

$$r_F = \sqrt{\lambda z_{\text{obs}}}, \quad (1)$$

where λ is the carrier wavelength. Normalizing W_{obs} by r_F provides a universal metric for obstruction severity, allowing our analysis to hold across different frequencies and deployment geometries.

2) *Normalized Range Separability*: Due to the finite aperture D , the array's ability to distinguish users in range is confined by a depth-of-focus (DOF) limit [18]. We define the range DOF as:

$$\Delta z_{\text{DOF}} \approx \frac{2\lambda z_1^2}{D^2}. \quad (2)$$

The normalized range separability μ is then:

$$\mu = \frac{\Delta z}{\Delta z_{\text{DOF}}}. \quad (3)$$

When $\mu \gg 1$, the users are resolvable in range; when $\mu \leq 1$, they fall within the same focal region, leading to significant interference.

B. Propagation and Effective Channel Model

1) *Fresnel Propagation*: We adopt the Fresnel diffraction integral to model the near-field propagation. Let $E_0(x')$ denote the electric field distribution (beamforming weights) at the aperture plane $z = 0$, where $x' \in [-D/2, D/2]$. The field propagated to a generic location (x, z) is given by (propagation prefactor omitted as it cancels in all channel coefficient ratios):

$$E(x, z) = \int_{-D/2}^{D/2} E_0(x') \exp\left(j \frac{2\pi}{\lambda} \frac{(x - x')^2}{2z}\right) dx'. \quad (4)$$

2) *Obstruction Modeling*: The finite obstruction at z_{obs} imposes a multiplicative mask $M(x)$ on the incident field:

$$M(x) = \begin{cases} 0, & |x| < W_{\text{obs}} \\ 1, & \text{otherwise} \end{cases}. \quad (5)$$

The propagation is modeled as a two-step process: the field first propagates from the aperture to the obstruction plane, is masked by $M(x)$, and then the surviving field propagates the remaining distance $(z - z_{\text{obs}})$ to the user locations.

C. Effective Channel, Precoding, and Metrics

1) *Effective MU Channel*: For a multi-user system serving $K = 2$ users, let \mathbf{w}_j denote the beamforming weight vector for the j -th user. The effective scalar channel coefficient h_{ij} between the j -th beamformer and the i -th user is defined as the complex field amplitude at the i -th user's location via the two-step Fresnel propagation with obstruction mask:

$$h_{ij} = E_{\mathbf{w}_j}(0, z_i), \quad \mathbf{H} = \begin{bmatrix} h_{11} & h_{12} \\ h_{21} & h_{22} \end{bmatrix} \in \mathbb{C}^{2 \times 2}. \quad (6)$$

Here h_{ij} represents the post-beamforming effective scalar channel, obtained by applying the N_{elem} -dimensional weight vector \mathbf{w}_j to the spatial channel and propagating through the obstruction model.

2) *ZF Common-SINR*: Zero-forcing (ZF) precoding is intentionally adopted as a worst-case linear precoder, as its performance is highly sensitive to channel conditioning. This choice clearly exposes the impact of Fresnel-zone blockage on noise amplification. The behavior under MMSE or regularized ZF precoding is outside the scope of this Letter. We adopt ZF precoding under a total power constraint P . The precoded signal vector is $\mathbf{x} = \beta \mathbf{H}^{-1} \mathbf{s}$, where \mathbf{s} contains the data symbols. The received signal is interference-free up to a common scaling factor β , leading to a symmetric SINR for both users:

$$\beta^2 = \frac{P}{\text{tr}((\mathbf{H}\mathbf{H}^H)^{-1})}, \quad \text{SINR} = \frac{\beta^2}{\sigma_n^2}. \quad (7)$$

3) *Metric and Protocol*: Our primary metric is the SINR gain:

$$\Delta \text{SINR}_{\text{dB}} = \text{SINR}_P - \text{SINR}_A, \quad (8)$$

where subscripts P and A denote the proposed Pearcey-inspired method and the baseline method, respectively. We fix $P = 1$ and the noise variance $\sigma_n^2 = 10^{-3}$ (normalized channel, consistent with [10]).

D. Fair Comparison Protocol

To ensure a rigorous evaluation of the proposed wavefront shaping, we adhere to the following fairness protocol:

- **Baseline:** Designs beams ignoring the obstruction, using standard free-space Green conjugate focusing toward each UE.
- **Pearcey (Proposed):** Designs beams ignoring the obstruction, using a calibrated quartic aperture phase.
- **Blind Calibration:** Any parameter tuning for the Pearcey-inspired quartic beam is performed in *free space* (assuming $M(x) = 1$), ensuring no knowledge of the obstruction is exploited.
- **Identical Evaluation:** Both methods are evaluated under the exact same obstruction model ($M(x)$ active) and power constraints.

III. PEARCEY-INSPIRED WAVEFRONT DESIGN AND CALIBRATION

To mitigate performance degradation caused by obstructions without relying on explicit obstruction knowledge, we propose a wavefront shaping strategy inspired by the Pearcey catastrophe integral. This section details the beam formulation, parameterization, and calibration procedure.

A. Baseline: Conventional Obstruction-Unaware Focusing

As a benchmark, we consider the standard near-field focusing beamforming designed for free-space propagation, corresponding to single-user maximum-ratio weights applied independently per user. The beamforming weight for the k -th user at aperture position $x \in [-D/2, D/2]$ is:

$$w_k^{(A)}(x) = \frac{1}{\sqrt{D}} \exp(j\Phi_{\text{focus}}(x; z_k)), \quad (9)$$

with the exact spherical focusing phase $\Phi_{\text{focus}}(x; z_k) = \frac{2\pi}{\lambda} \sqrt{x^2 + z_k^2}$. This baseline represents the optimal strategy in the absence of obstructions but lacks robustness when the Fresnel zone is partially blocked.

B. Pearcey-Inspired Quartic Wavefront

Diffraction catastrophe theory suggests that specific higher-order phase polynomials can generate structurally stable wave packets [16]. The Pearcey integral, governed by a fourth-order phase term, produces a cusped caustic structure known for its stability [17]. Inspired by this, we modify the conventional focusing phase by injecting a quartic phase term. The proposed Pearcey-inspired quartic beamforming weight $w_k^{(P)}(x)$ is:

$$w_k^{(P)}(x) = \frac{1}{\sqrt{D}} \exp(j [\Phi_{\text{focus}}(x; z_k) + \delta a_2 x^2 + \alpha_4 x^4]), \quad (10)$$

where $\alpha_4 x^4$ introduces the Pearcey-like quartic structure, and $\delta a_2 x^2$ is an auxiliary quadratic term used solely for calibration (see Sec. III-D).

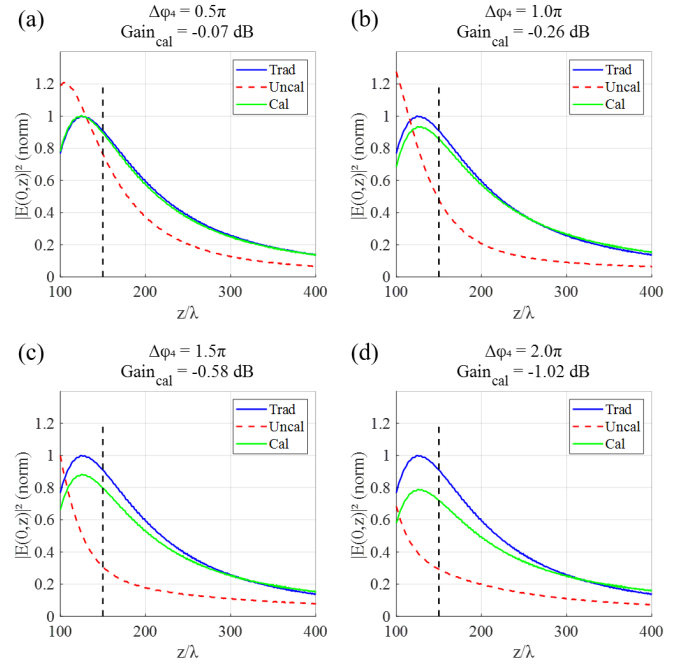


Fig. 2. Free-space axial intensity profiles ($|E(0,z)|^2$) of the calibrated Pearcey-inspired quartic beam under varying quartic phase strengths $\Delta\phi_{4,\text{edge}} \in \{0.5\pi, \pi, 1.5\pi, 2\pi\}$, normalized to the diffraction-limited baseline peak (blue solid). The blind calibration successfully aligns the focus to $z_1 = 150\lambda$ for all cases. As the edge phase swing increases to 2π , the peak intensity exhibits a progressive penalty (≈ 1.0 dB), reflecting the energy redistribution into the caustic wings that confers self-healing capability.

C. Design Insight: Normalization and Parameterization

A fixed quartic coefficient α_4 would produce inconsistent caustic structures for users at different ranges due to varying Fresnel numbers. To ensure consistent topological structure for all users, we parameterize the quartic strength via the *edge phase swing*, defined as the total quartic phase accumulation at the aperture boundary ($x_{\text{edge}} = \pm D/2$):

$$\Delta\phi_{4,\text{edge}} \triangleq \alpha_4 (D/2)^4 \Rightarrow \alpha_4 = \frac{\Delta\phi_{4,\text{edge}}}{(D/2)^4}. \quad (11)$$

Design Choice: We select $\Delta\phi_{4,\text{edge}} = 2\pi$ based on the trade-off between on-axis efficiency and structural stability. This value corresponds to a full phase cycle at the aperture edge, which is sufficient to induce a stable cusp caustic without severe destructive interference along the propagation axis. As shown in Fig. 2, setting $\Delta\phi_{4,\text{edge}} = 2\pi$ limits the free-space gain penalty to approximately 1.0 dB. Smaller values (e.g., $\Delta\phi_{4,\text{edge}} = 0.5\pi$) yield a negligible gain penalty but fail to induce a meaningful caustic structure, producing no practical self-healing benefit in blocked scenarios.

D. Free-Space Calibration and Gain-Robustness Trade-off

1) *The “Focus Shift” Challenge:* Adding a quartic phase term $\alpha_4 x^4$ inherently shifts the effective focal length due to finite aperture effects. Without correction, the beam focus would shift significantly toward the aperture, invalidating any direct comparison with the baseline. To resolve this, we introduce a **Blind Free-Space Calibration** step. The auxiliary

quadratic parameter δa_2 in (10) is tuned to maximize the on-axis intensity at the user's nominal location z_k under free-space propagation:

$$\delta a_2^* = \arg \min_{\delta a_2} \left(- \left| E_{\mathbf{w}_k^{(P)}}(0, z_k) \right|_{M=1} \right)^2, \quad (12)$$

where $E_{\mathbf{w}_k^{(P)}}(0, z_k)|_{M=1}$ denotes the on-axis field at z_k obtained by propagating $w_k^{(P)}(x; \delta a_2)$ through the free-space Fresnel propagator (4) with $M(x) = 1$. This optimization is obstruction-unaware by construction.

2) *Gain vs. Robustness Trade-off*: Fig. 2 visualizes the calibration results for different quartic strengths. As $\Delta\phi_{4,\text{edge}}$ increases from 0.5π to 2π , the calibrated beam maintains its focus near z_1 , but the peak intensity gradually decreases (from -0.07 dB to -1.02 dB relative to baseline). This energy is not dissipated; it is spatially redistributed into the wings of the Pearcey caustic structure. This redistribution is precisely the mechanism that confers **self-healing capability**: even when the central Fresnel zones are blocked, the energy distributed in the marginal aperture areas coherently reconstructs the focal field. This structural stability preserves the **spatial signature** of the user channel, thereby maintaining channel rank and mitigating the severe noise amplification inherent to ZF precoding in blocked scenarios.

IV. NUMERICAL RESULTS AND DISCUSSION

We evaluate the proposed Pearcey-inspired beamforming strategy using the fairness protocol defined in Sec. II-D. The system parameters are $N_{\text{elem}} = 64$, $d = 0.49\lambda$, $z_1 = 150\lambda$, $\eta = 0.5$, $\sigma_n^2 = 10^{-3}$, and $P = 1$. Results for the obstruction position $\eta = 0.5$ are representative; varying η affects the absolute threshold values while preserving the qualitative advantage structure, which is deferred to future work.

A. Impact of Obstruction Size

Fig. 3 plots the SINR gain and the channel condition number ratio as a function of W_{obs}/r_F for $\mu \in \{0.5, 1.0, 2.0\}$.

A critical finding is the existence of a clear **advantage threshold**. In the unobstructed regime ($W_{\text{obs}} \rightarrow 0$), the baseline outperforms the Pearcey-inspired quartic beam by approximately 1.0 dB, consistent with the free-space calibration penalty shown in Fig. 2. This confirms that for pure LoS channels, perfect Green's function focusing is optimal.

As obstruction size increases, the baseline degrades rapidly due to loss of the main Fresnel zones essential for focus. The Pearcey-inspired quartic beam exhibits resilience via its distributed caustic energy. The exact 0 dB crossover thresholds, extracted by linear interpolation from the simulation data, are $W_{\text{obs}}/r_F = 0.42$ ($\mu = 0.5$), 0.57 ($\mu = 1.0$), and 0.32 ($\mu = 2.0$). The non-monotonic ordering of these values reflects the axial Fresnel periodicity of the cross-channel term h_{12} : as Δz varies, finite-aperture diffraction produces quasi-periodic oscillations in the channel conditioning with a period of approximately Δz_{DOF} (equivalently, $\Delta\mu \approx 1$). The mean advantage threshold therefore lies near $W_{\text{obs}}/r_F \approx 0.35$ – 0.45 , with local fluctuations of amplitude $\sim \pm 0.1$ due to this Fresnel periodicity.

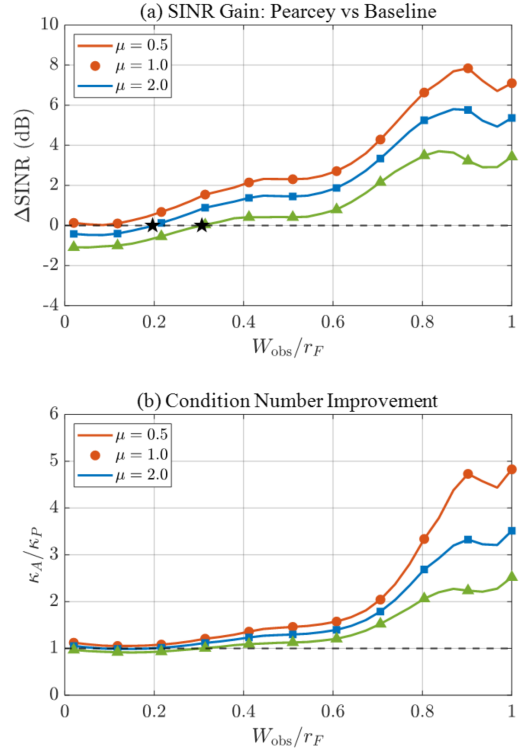


Fig. 3. Performance comparison versus normalized obstruction width W_{obs}/r_F for $\mu \in \{0.5, 1.0, 2.0\}$. (a) Common SINR gain $\Delta\text{SINR}_{\text{dB}}$ of the Pearcey-inspired quartic beam over baseline, with star markers (★) indicating the exact 0 dB crossover thresholds extracted by linear interpolation. (b) Channel condition number ratio κ_A/κ_P , illustrating how the Pearcey wavefront mitigates ill-conditioning caused by Fresnel-zone blockage.

Fig. 3(b) confirms the underlying mechanism: the condition number ratio κ_A/κ_P grows monotonically with obstruction size for all μ values, indicating that the Pearcey-inspired quartic phase consistently preserves better channel orthogonality than the truncated spherical wavefront under blockage. At large obstruction ($W_{\text{obs}}/r_F \rightarrow 1$), the ratio reaches $\kappa_A/\kappa_P \approx 3$ – $5\times$, corresponding to the dominant SINR gain regime. The larger κ_A/κ_P observed for $\mu = 1.0$ relative to $\mu = 0.5$ at high blockage arises because conventional focusing at $\mu = 1.0$ already operates near the resolvability limit, making it more susceptible to Fresnel-zone distortion and thus more sensitive to the stabilizing effect of the quartic phase.

B. Advantage Map

Fig. 4 presents a heatmap of the SINR gain over the $(\mu, W_{\text{obs}}/r_F)$ plane. Two distinct regimes are evident.

First, a prominent *sweet spot* emerges for strong Fresnel-core blockage ($W_{\text{obs}}/r_F \gtrsim 0.75$) combined with low user separability ($\mu \lesssim 0.6$), where the Pearcey-inspired quartic wavefront yields gains exceeding 5 dB and peaking at 8.5 dB. Second, for moderate obstruction ($W_{\text{obs}}/r_F \approx 0.4$ – 0.7) across a wide range of μ , consistent gains of 2–4 dB are observed, demonstrating broad practical utility. For well-separated users ($\mu \gtrsim 2$), the advantage diminishes as the baseline inherently recovers orthogonality through sufficient range resolution.

This gain is fundamentally driven by the stabilization of the ZF inversion. Partial Fresnel-zone blockage causes the conven-

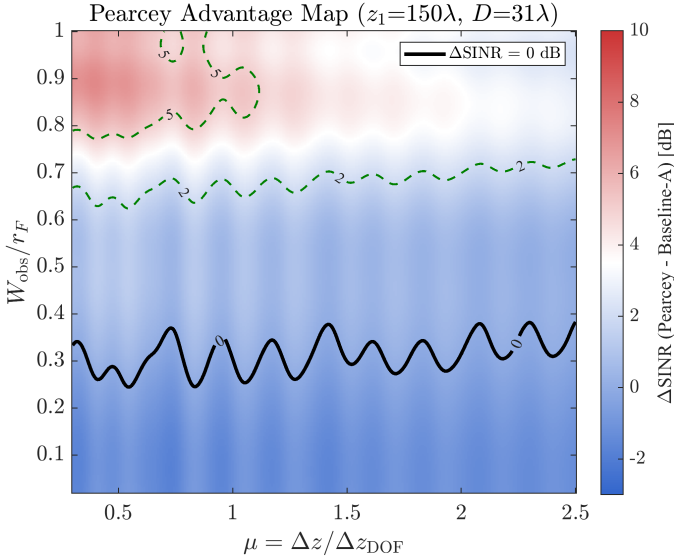


Fig. 4. Heatmap of the SINR advantage ($\Delta\text{SINR}_{\text{dB}}$) of the proposed Pearcey-inspired quartic beam over baseline, over the $(\mu, W_{\text{obs}}/r_F)$ plane. The bold black contour is the 0 dB break-even boundary; green dashed contours mark the 2, 5, and 8 dB levels. A mild Gaussian smoothing ($\sigma = 1.5$ grid units) is applied to the displayed heatmap to reveal the underlying trend; residual oscillation of the 0 dB contour along the μ axis reflects the axial Fresnel periodicity discussed in Sec. IV.A.

tional channel vectors of co-angular users to become highly collinear, spiking the condition number and amplifying noise via the ZF scaling factor $\beta^{-2} \propto \text{tr}((\mathbf{H}\mathbf{H}^H)^{-1})$. By preserving distinct range signatures under blockage, the calibrated quartic phase mitigates the degradation of the channel's smallest singular value. This conditioning improvement significantly outweighs the focal-gain penalty of the quartic term in the dominance regime. Conversely, when obstruction is negligible, the conventional focusing remains near-optimal; the blind calibration ensures the proposed method converges to within 1.0 dB of the baseline rather than inducing artificial losses.

V. CONCLUSION

This letter proposed an obstruction-unaware wavefront shaping strategy using Pearcey-inspired quartic phase profiles to enhance multi-user RNF connectivity. By implementing a blind free-space calibration, the proposed method corrects intrinsic focal shifts while preserving the resilience of diffraction catastrophes. Numerical results reveal a well-defined advantage region governed jointly by the Fresnel-normalized obstruction width and the user range separability. Specifically, the quartic wavefront significantly mitigates zero-forcing noise amplification when strong Fresnel-core blockage coincides with users near the depth-of-focus limit ($\mu \lesssim 0.6$, $W_{\text{obs}}/r_F \gtrsim 0.75$), yielding gains up to 8.5 dB. Future work will investigate

the adaptive tuning of the quartic strength and the extension to two-dimensional apertures and three-dimensional propagation geometries.

REFERENCES

- [1] M. Cui, Z. Wu, Y. Lu, X. Wei, and L. Dai, "Near-field MIMO communications for 6G: Fundamentals, challenges, potentials, and future directions," *IEEE Commun. Mag.*, vol. 61, no. 1, pp. 40–46, Jan. 2023.
- [2] X. You, C. Wang, J. Huang, X. Gao, C. Zhang, M. Wang *et al.*, "Towards 6G wireless communication networks: vision, enabling technologies, and new paradigm shifts," *Sci. China Inf. Sci.*, vol. 64, no. 1, Art. no. 110301, 2021.
- [3] H. Zhang, N. Shlezinger, F. Guidi, D. Dardari, and Y. C. Eldar, "6G wireless communications: From far-field to near-field," *IEEE Wireless Commun.*, vol. 61, no. 4, pp. 72–77, April 2023.
- [4] Z. Wu and L. Dai, "Multiple access for near-field communications: SDMA or LDMA?" *IEEE J. Sel. Areas Commun.*, vol. 41, no. 6, pp. 1918–1935, Jun. 2023.
- [5] Z. Wang *et al.*, "Extra-large-scale MIMO: Fundamentals, challenges, and future directions," *IEEE Wireless Commun.*, vol. 31, no. 3, pp. 117–124, June 2024.
- [6] M. Alrabeiah and A. Alkhateeb, "Deep learning for mmWave beam and blockage prediction using sub-6 GHz channels," *IEEE Trans. Commun.*, vol. 68, no. 9, pp. 5504–5518, Sept. 2020.
- [7] Y. Yang, S. Dang, M. Wen, B. Ai, and R. Qingyang Hu, "Blockage-aware robust beamforming in RIS-aided mobile millimeter wave MIMO systems," *IEEE Trans. Wireless Commun.*, vol. 23, no. 11, pp. 16906–16921, Nov. 2024.
- [8] M. Hou, Y. Qin, J. Chen, L. Zhang, L. Song, and S. Gao, "A multi-dimensional multiplexing intelligent omni-surface: Principles and experiments," *IEEE Wireless Commun.*, early access, 2025.
- [9] I. V. A. K. Reddy, D. Bodet, A. Singh, V. Petrov, C. Liberale, and J. M. Jornet, "Ultrabroadband terahertz-band communications with self-healing Bessel beams," *Commun. Eng.*, vol. 2, no. 1, p. 70, Oct. 2023.
- [10] Y. Qin, J. Chen, Z. Jiang, Z. Chen, and Y. Huang, "Exploiting non-diffracting beams for resilient near-field millimeter-wave communications: A quantitative roadmap," arXiv preprint arXiv:2510.14858, Oct. 2025. [Online]. Available: <https://arxiv.org/abs/2510.14858>
- [11] D. Bodet, V. Petrov, S. Petrushkevich, and J. M. Jornet, "Sub-terahertz near field channel measurements and analysis with beamforming and Bessel beams," *Sci. Rep.*, vol. 14, art. no. 19675, Aug. 2024.
- [12] H. Guerboukha, B. Zhao, Z. Fang, E. Knightly, and D. M. Mittleman, "Curving THz wireless data links around obstacles," *Commun. Eng.*, vol. 3, no. 1, p. 58, Mar. 2024.
- [13] D. Darsena, F. Verde, M. Di Renzo, and V. Galdi, "Airy beams for near-field communications: Fundamentals, potentials, and limitations," arXiv preprint arXiv:2508.13714, Aug. 2025. [Online]. Available: <https://arxiv.org/abs/2508.13714>
- [14] A. Liu, W. Mei, P. Wang, D. Wang, Y. Wu, Z. Chen, and B. Ning, "Near-field THz bending beamforming: A convex optimization perspective," arXiv preprint arXiv:2503.20274, Mar. 2025.
- [15] W. Zhao, S. Abadal, G. Song, J. Jiang, and C. Han, "Terahertz wireless data center: Gaussian beam or Airy beam?" *IEEE Trans. Wireless Commun.*, Early Access, 2025.
- [16] J. D. Ring, J. Lindberg, A. Mourka, M. Mazilu, K. Dholakia, and M. R. Dennis, "Auto-focusing and self-healing of Pearcey beams," *Opt. Express*, vol. 20, no. 17, pp. 18955–18966, Aug. 2012.
- [17] T. Cao, S. Jin, Q. Chen, P. Ma, S. A. Ponomarenko, Y. Cai, C. Liang, and J. Liu, "Diffraction-free partially coherent Pearcey beam," *Opt. Express*, vol. 33, no. 2, pp. 1827–1835, Jan. 2025.
- [18] E. Björnson and L. Sanguinetti, "Power scaling laws and near-field behaviors of massive MIMO and intelligent reflecting surfaces," *IEEE Open J. Commun. Soc.*, vol. 1, pp. 1306–1324, 2020.